Chapter 7

Differential Mg^{2+} Deposition on DNA Holliday Junctions Dictates the Rate and Stability of Conformational Exchange †

†This work is currently under review. "Differential Mg^{2+} Deposition on DNA Holliday Junctions Dictates the Rate and Stability of Conformational Exchange" ***Pratibha Agarwala***, *Arumay Pal, Milan Kumar Hazra*, and Dibyendu K. Samsal**

In this chapter, we discuss our work investigating the kinetic choreography and preferential stability of HJ conformations under ionic conditions that closely mimics physiological environment relevant to cellular biology.

7.1 Introduction

The open planar structure of the HJ accelerates the branch migration and resolvase activities and also helps in exchanging the genetic material.[261, 282-283] Not only the stacked conformation but also open state conformation may be populated even at high ion concentrations and while the transition from two stacked conformations occurs.[275] The open state dynamics plays a pivotal role in resolution of HJ through the enzyme recognition process, it's also a crucial intermediate in the branch migration process for the mobile HJ.[248, 284] A clear understanding of the intrinsic conformation properties of HJ is crucial for cellular processing. This information has paramount importance in terms of homologous recombination in the genetic reshuffling process as it exploits the dynamic nature of HJ.[285]

Present study aims to address the coordinated thermodynamic and kinetic choreography of conformational transitions in HJ using the smFRET and MD simulations at different ionic concentrations. More importantly, we aim to decode the effect of near-physiological divalent ion concentration on HJ dynamics. A three-state kinetic model ensures best fit to the conformational exchange mechanism. We have obtained newer kinetic information employing multi-order time-correlation approach blended with kinetic network model to decode the transition rates and mapped the same on the free-energy landscape obtained from smFRET trajectories. Coarse grained MD simulations predict differential counter-ion condensation at junction center and strand regimes of HJ and may dictate or bias conformational exchange.

7.2 Method

7.2.1 Coarse-grained and All-atom Simulation Methodology

In order to access the structural ensemble of DNA HJ, we have employed a coarse-grained structure-based model of nucleic acids with all-atom resolution. The potential energy function has been defined as

$$E = \sum_{\text{Bonds}} k_{\text{Bonds}}(r_i - r_{i,0})^2 + \sum_{\text{Angles}} k_{\text{Angles}}(\theta_i - \theta_{i,0})^2 + \sum_{\text{Impropers}} k_{\text{Impropers}}(\chi_i - \chi_{i,0})^2 + \sum_{\text{Planars}} k_{\text{Planars}}(\chi_i - \chi_{i,0})^2 + \sum_{\text{Backbone}} k_{\text{Backbone}} F_D(\phi)(\phi_i - \phi_{i,0}) + \sum_{\text{Contacts}} \varepsilon_C \left[\left(\frac{\sigma_{ij}}{r_{ij}}\right)^{12} - 2\left(\frac{\sigma_{ij}}{r_{ij}}\right)^{6}\right] + \sum_{\text{Non-Contacts}} \varepsilon_{NC} \left[\left(\frac{\sigma_{NC}}{r_{ij}}\right)^{12}\right] + K_{\text{Coulomb}} B(\kappa) \sum_{i,j} \frac{q_i q_j e^{-\kappa r_{ij}}}{\varepsilon_{Solvent} r_{ij}}$$

Where, $F_D(\phi) = [1 - \cos(\phi)] + 0.5[1 - \cos(3\phi)]$ (7.1)

The first five terms represent bonded, angular, proper and improper dihedral potentials. $r_{i,0}, \theta_{i,0}, \chi_{i,0}, \phi_{i,0}$ represent equilibrium bond-length, angle, proper and improper dihedrals and backbone dihedrals respectively and has been obtained from provided structure. Short-range native interactions have been modelled as LJ potential whereas non-native ones interact with purely repulsive interactions such that the atoms do not overlap on each other. σ_{ij} represents distance between atoms i and j centre of mass while being in contact and ε_C denotes contact strength. Electrostatics have been described with Debye-Hückel model.
The parameters were set to the following values:

$$k_{\text{Bonds}} = \frac{50\varepsilon}{\text{Å}^2}, k_{\text{Angles}} = \frac{40\varepsilon}{\text{rad}^2}, k_{\text{Impropers}} = \frac{5\varepsilon}{\text{rad}^2}, k_{\text{Planars}} = \frac{20\varepsilon}{\text{rad}^2}, \varepsilon_{NC} = 0.1\varepsilon, \sigma_{NC} = 2.5\text{Å}, \varepsilon = 1.0$$

Timestep of 0.0005 has been used for solving the Langevin dynamics. Simulations has been performed Gromacs version 515[286] while SMOG (structure based model for biomolecules)[287-290] has been used to generate the topology and coarse-grained (CG) structures. Solvent has been treated as an implicit dielectric medium with dielectric constant 80. Divalent salt $MgCl_2$ has been introduced explicitly in addition to a 50 mM NaCl implicit buffer. However, due to coarse resolution of our model in the absence of solvent, we have calibrated charge of ions through the computation of radial distribution of ions around DNA HJ in our CG model and compared the same with all-atom explicit solvent 200ns simulation (production run) of HJ at 200 mM $MgCl_2$ at temperature 300K.

For explicit solvent all-atom simulations, we have used Amber OL21 forcefield for DNA and SPC/E water with ions234lm_1264_spce parameter set for divalent Mg^{2+}. Octahedral box has been used where DNA HJ was placed such that any atom on DNA HJ stays at least 1.6 nm away from surface of the box. Equation of motions were integrated with a timestep of 2 fs in NPT ensemble for the production run.

Upon running coarse-grained simulations with gradually decreasing Mg^{2+} and Cl^- charges, we have observed the radial distribution of Mg^{2+} around HJ significantly matches with all-atom explicit solvent simulations for ionic charges of Mg^{2+} =1.2 and Cl^-=0.6 in our coarse-grained model (Figure 7.1).

We validated our RDF profiles by comparing them with prior atomistic simulations. The pronounced initial peak at approximately 0.25 nm in our all-atom RDF aligns with the inner-sphere Mg^{2+} binding seen in Wheatley et al.[291], whereas the more diffuse second peak pertains to outer-sphere interactions. Moreover, our results align with the Mg^{2+}-dependent junction stability documented by Zhang et al.,[248] reinforcing the physical validity of our hypothesis.

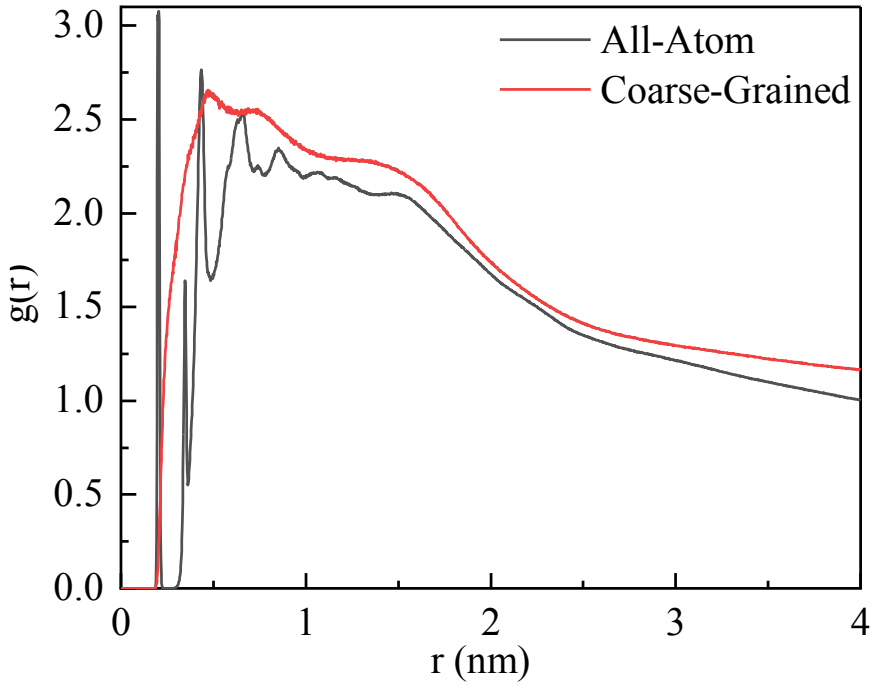


Figure 7.1 Radial distribution function of positively charged Mg^{2+} ions around negatively charged DNA HJ at near physiological salt concentration 200mM obtained from all-atom explicit solvent simulation with Amber forcefield and TIP4P water (black) and from coarse-grained structure-based model in absence of solvent with continuum dielectric medium 80 (red).

Table 7.1 The sequence of ssDNA with the chain ID used for MD simulation.

Chain ID	**Sequence**
A (cyan) (Cy3 labelled in experiment)	5′-CCG TAG CAG CGC GAG CGG TGG G-3′
B (yellow) (Cy5 labelled in experiment)	5′-CCC TAG CAA GCC GCT GCT ACG G-3′
C(Magenta)	5′-CCC AGT TGA GCG CTT GCT AGG G-3′
D(green) (biotin labelled in experiment)	5′-CCC ACC GCT CGG CTC AAC TGG G-3′

The electrostatic interactions between DNA HJ and ions and intra-DJ repulsions has been quantified by Debye-Hückel continuum electrostatics[292] [Equation 7.1] q_i and q_j denote the charge of the i^{th} and j^{th} bead, inter-bead distance has been denoted as r_{ij}, $\varepsilon_{Solvent}$ denotes the solvent dielectric constant, and $K_{Coulomb} = 4\pi\varepsilon_0$ =332 kcal/mol. B(κ) was dependent on salt concentration and the radius (a) of ions produced by the dissociation of the salt, and was given by $B(\kappa) = \frac{e^{\kappa a}}{1+e^{\kappa a}}$. According to Debye-Hückel theory, electrostatic interactions of an ion ranges upto a distance of the order of κ^{-1}, which is called Debye screening length. The Poisson-Boltzmann equation leads to the following relation of κ to ionic strength, $\kappa^2 = \frac{8\pi N_A e^2 \rho_A I}{1000 \varepsilon_{Solvent} k_B T}$; where N_A represent the Avogadro number, e is charge of an electron, ρ_A denotes solvent density, I represent ionic strength of the medium, k_B is the Boltzmann constant, and T is the temperature

in reduced units. DNA HJ was placed in a cubic box of dimensions 15 × 15 × 15 nm. At each temperature and salt concentration, multiple independent trajectories has been generated solving Langevin equation in an NVT ensemble.

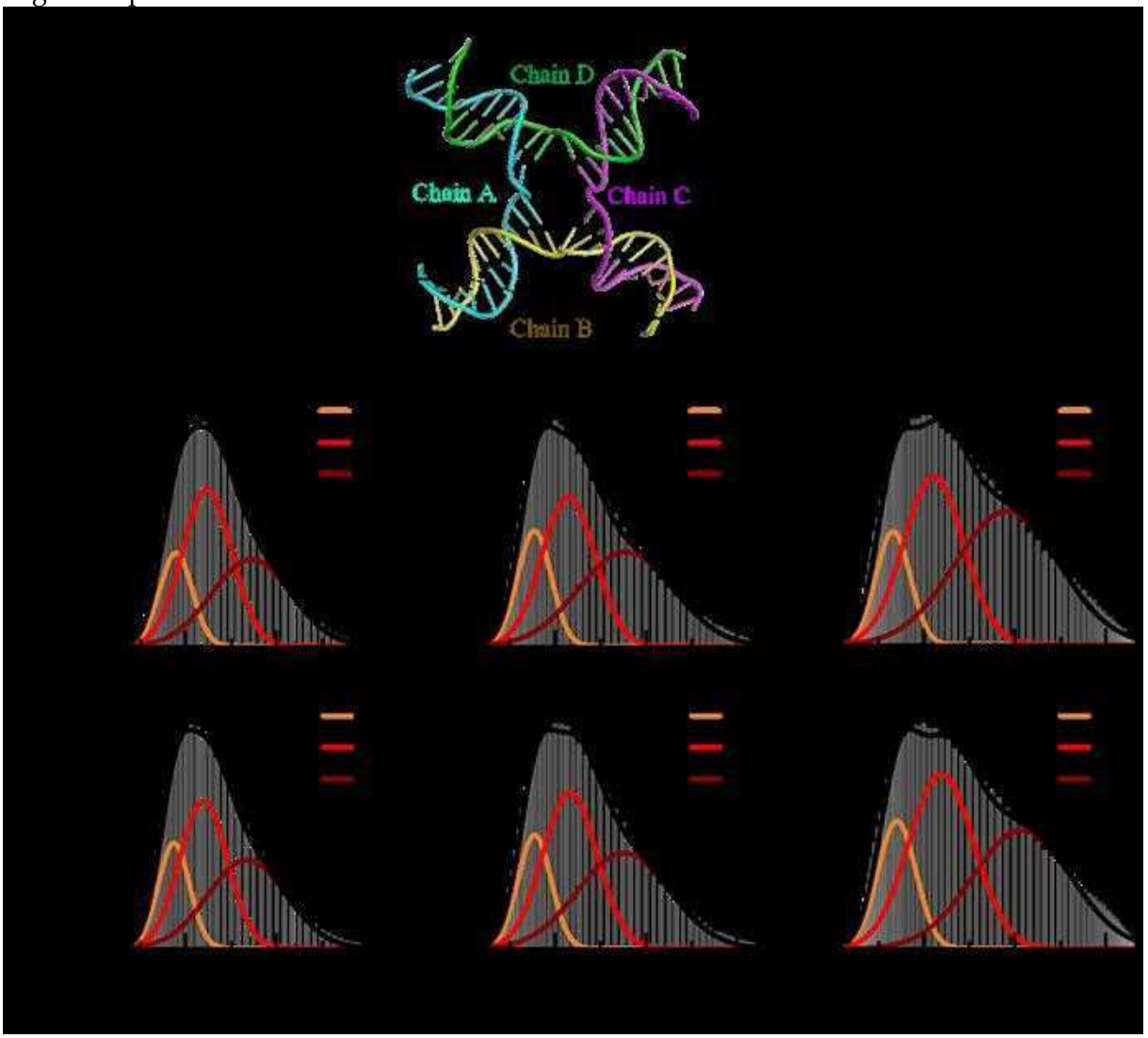


Figure 7.2 (A) Schematic diagram of HJ shows that the FRET efficiency was calculated by considering the distance of chain A 5' position to chain B 5' position as per the Table 7.1. (B-D) Probability Density of FRET efficiency calculated from the MD simulation trajectory shows three prominent states corresponding to $\mathbf{E_{FRET}}$ in presence of 50 mM Mg^{2+} at 60K, 75K and 90K respectively. (E-G) Probability Density of FRET efficiency calculated from the MD simulation trajectory shows three prominent states corresponding to $\mathbf{E_{FRET}}$ in presence of 200 mM Mg^{2+} at 60K, 75K and 90K respectively. Based on FRET efficiency and conformational features, state S1 corresponds to the stacked-X isoI form, S2 represents the open conformation, and S3 corresponds to the stacked-X isoII form.

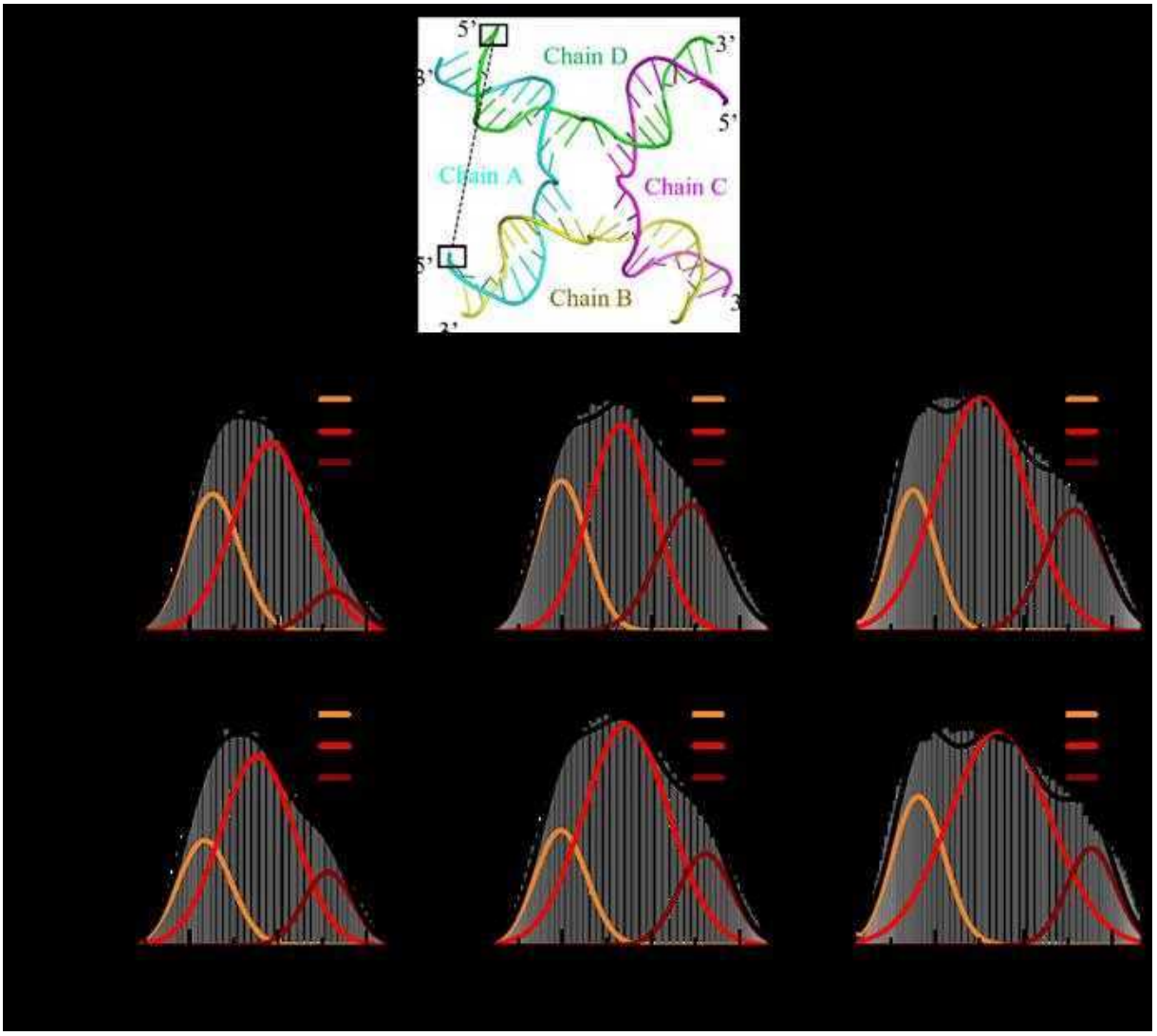


Figure 7.3 (A) Schematic diagram of HJ shows that the FRET efficiency was calculated by considering the distance of chain A 5' position to chain D 5' position as per the Table 7.1. (B-D) Probability Density of FRET efficiency calculated from the MD simulation trajectory shows three prominent states corresponding to $\mathbf{E_{FRET}}$ in the presence of 50 mM Mg^{2+} at 60K, 75K and 90K, respectively. (E-G) Probability Density of FRET efficiency calculated from the MD simulation trajectory shows three prominent states corresponding to $\mathbf{E_{FRET}}$ in the presence of 200 mM Mg^{2+} at 60K, 75K and 90K, respectively. Based on FRET efficiency and conformational features, state S1 corresponds to the stacked-X isoI form, S2 represents the open conformation, and S3 corresponds to the stacked-X isoII form.

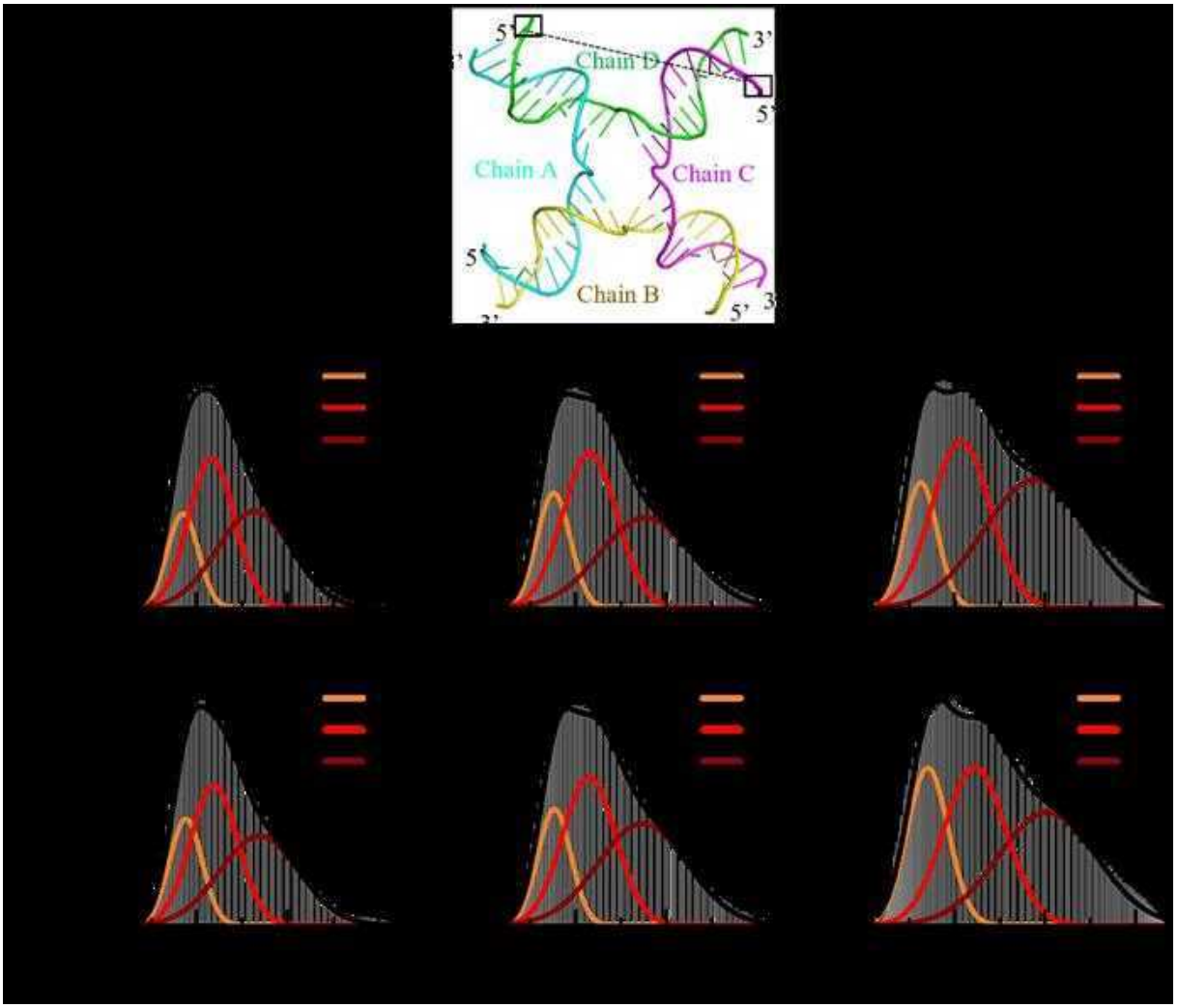


Figure 7.4 (A) Schematic diagram of HJ shows that the FRET efficiency was calculated by considering the distance of chain C 5' position to chain D 5' position as per the Table 7.1. (B-D) Probability Density of FRET efficiency calculated from the MD simulation trajectory shows three prominent states corresponding to $\mathbf{E_{FRET}}$ in the presence of 50 mM Mg^{2+} at 60K, 75K and 90K, respectively. (E-G) Probability Density of FRET efficiency calculated from the MD simulation trajectory shows three prominent states corresponding to $\mathbf{E_{FRET}}$ in the presence of 200 mM Mg^{2+} at 60K, 75K and 90K, respectively. Based on FRET efficiency and conformational features, state S1 corresponds to the stacked-X isoI form, S2 represents the open conformation, and S3 corresponds to the stacked-X isoII form.

7.3 Results & Discussion

7.3.1 smFRET from DNA HJ Shows Real-Time Dynamic Transition of States in Millisecond Time-Scale

Mg^{2+} ion plays a critical role in the dynamic conformational change of DNA HJ, which are key intermediate structure during DNA recombination and repair processes.[275] HJs are formed during genetic recombination when two DNA duplexes exchange strands. The four arms of the junction can adopt several conformations, including stacked-X, and open-X structures.[293] Mg^{2+} ions are essential for stabilizing the HJ structure by coordinating and neutralizing the negative charges of phosphate ion in DNA backbone, which helps in counteracting the repulsion between

the negatively charged DNA strands. This stabilization is particularly important during the transition between different conformations of the HJ. Furthermore, Mg^{2+} ions facilitate the dynamic conformational changes of HJs by promoting strand exchange reactions.

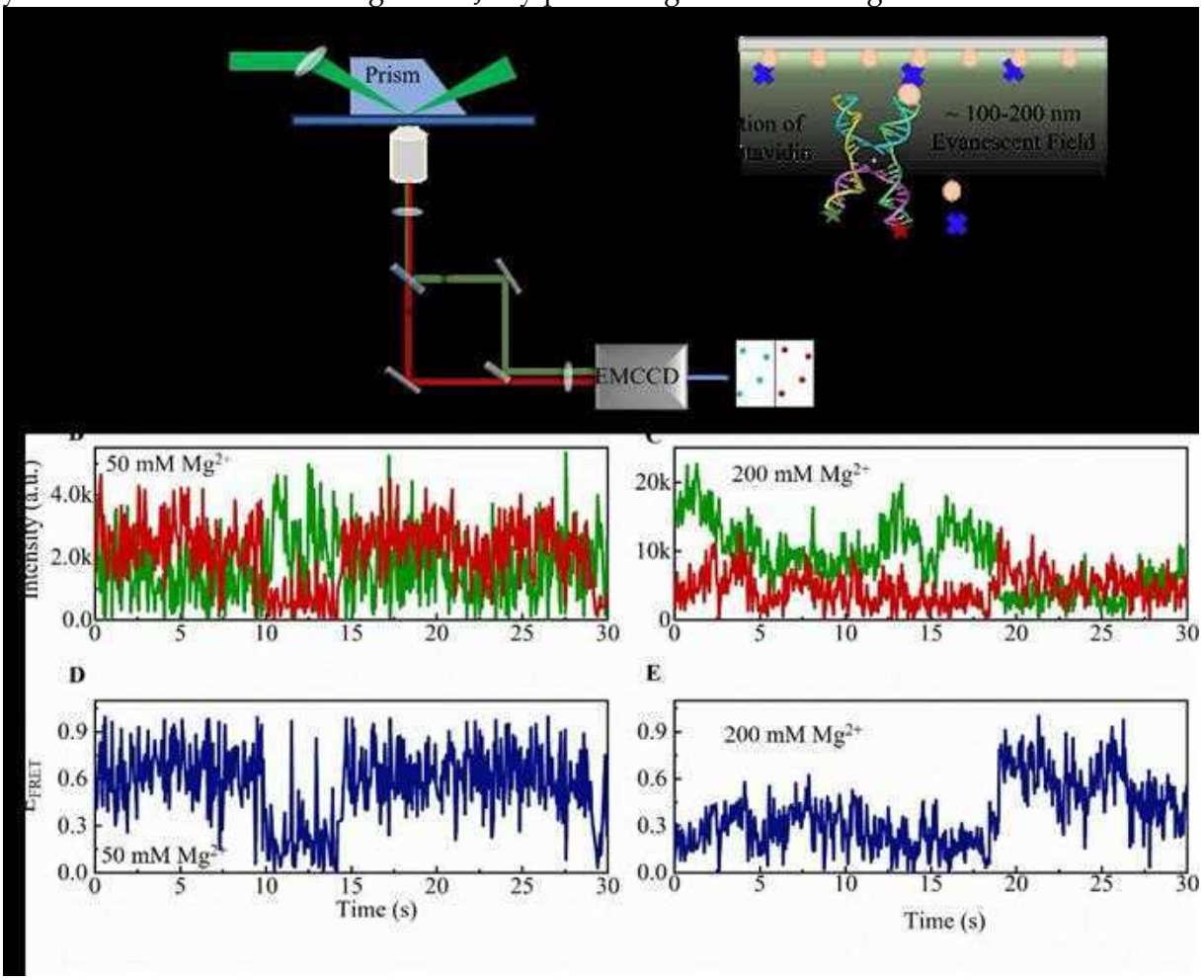


Figure 7.5 (A) A schematic representation of custom build prism-based total internal reflection fluorescence (pTIRF) microscope to study smFRET. The excitation beam of 559 nm laser enters to the prism through a biconvex lens of 200 mm focal length. When the beam approaches the interface of quartz slide and aqueous sample at the incident angle higher than the critical angle, this results total internal reflection which create an evanescent field of 100-200 nm depth into the sample. The emission signal passes through the 100X objective and enters Optosplit-II, where dichroic mirror (Chroma: ZT633rdc-UF2), was used to separate signals, and then bandpass filters (BP) - ET585/65m and ET706/95m were used to cleanup signals for donor and acceptor respectively. Right hand side shows large version of the sample chamber which shows how HJ is immobilized on the glass surface by Biotin-BSA and Streptavidin. Sequences of DNA oligos are given in Table 7.1. (B-C) Representative single-molecule fluorescence intensity time-trajectories of Cy3 (Donor, Green) and Cy5 (Acceptor, Red) recorded from one single DNA HJ in presence of 50 mM and 200 mM Mg^{2+} ion. The anticorrelated pattern of two signals is a clear signature of smFRET. (D-E) FRET efficiency fluctuation (blue line) calculated from the respective data shown in Figure B and C.

During recombination, the junction undergoes structural transitions, including branch migration and resolution, where Mg^{2+} ions help in facilitating the movement of DNA strands and resolving the junction into two separate duplex molecules.[275, 294] Moreover, Mg^{2+} ions can influence the specificity and efficiency of recombination reactions by affecting the kinetics and thermodynamics of the strand exchange process. They can also mediate the interactions between

the proteins involved in recombination, such as recombinases and resolvases, and the DNA substrate. Thus, it is essential to understand the Mg^{2+} dependence on the dynamics and kinetics of DNA conformational change of states in real-time. To do that, we applied state-of-the-art prism-type TIRF microscopy to calculate efficiency of single-molecule fluorescence resonance energy transfer in real time. FRET efficiency is inversely proportional to 6th power of the distance between donor and acceptor molecule (Equation 3.8), so when there is a high FRET efficiency, we can consider that the two arms of HJ are close to each other forming a stacked conformation.

The dynamic nature of conformational change is evident from the fluctuations of FRET efficiency in the Figure 7.5 which was derived from the anti-correlated signal fluctuation of the donor (Cy3) and acceptor (Cy5) present in a single HJ molecule. This experiment was performed with 50 ms camera exposure time which is in the same order of conformational exchange time to it's sub-states or intermediate states. The reason for performing experiments with two different Mg^{2+} ion concentration is that, taking an in-situ concentration of 50 mM will give a pattern of dynamics near or below physiological concentration, whereas 200 mM will give a dynamics pattern in a high abundance of ionic spheres. Although there is various report which says a long range of presence of Mg^{2+} ions in cellular environment. It is thought to be essentially a tough experiment to determine Mg^{2+} considering all physiological environment at an artificial condition. Here we show that conformational fluctuation in real-time in presence of both concentrations. The donor and acceptor are fluctuating in the anticorrelated pattern reveals that the fluctuations in the intensity trajectory is due to the energy transfer from the donor to acceptor molecule indicating dynamic conformational change. HJ shows much more dynamical pattern of conformational dynamics in presence of 50 mM of Mg^{2+} (Figure 7.5.B) compared to the 200 mM Mg^{2+}(Figure 7.5.D), which is due to more stable DNA HJ phosphate backbone in presence of higher concentration of positive ion that neutralizes the negatively charged phosphate ions. The change in ion concentration leads to the different dynamic aspects of HJ in stacked and unstacked conformation which we will investigate in the next section. However, the dynamics leading to various conformational state including intermediate states and exchange rate with thermodynamic parameters are revealed from further stational data analysis.

7.3.2 State Conformation Transition Dynamics in DNA HJ Revealed by smFRET Experiment and TCF Analysis, MD simulation for Exact Quantification of Thermodynamic Feasibility

HJ undergoes multiple short-lived conformational states (macro-state) including intermediate states during conformational interchange dynamic cycle, which ultimately determines and select the route for DNA recombination and repair processes. Thus, it is important to know the thermodynamically stable conformational states at different cellular conditions, namely ionic environment or temperature, which is extremely difficult to determine by conventional ensemble-averaged optical methods. Here, we applied statistical calculation methods on FRET efficiency time-trajectories to determine the most stable thermodynamic structures, which is again supported by MD simulation. Previously, there are various reports on the number of states that are present during the dynamics of HJ. Considering a HJ can go through N number of conformational states at a constant temperature of T, the probability of occurrence of i^{th} conformation is given by Boltzmann distribution, which is,

$$p_i = (1/Z)e^{-G_i/k_BT} \qquad (7.2)$$

Where k_B is Boltzmann's constant, G_i is the Gibbs free energy of the i^{th} conformation and $Z = \sum_{i=1}^{N} e^{-G_i/k_BT}$, which is partition function. In addition, the probability will be unity at the normalized condition. Individual HJ conformational state (Figure 7.6.A) is expected to have a lifetime as well as interconvert in tens of milli-second timescale, which is much above our resolution of smFRET experiment that means the observed fluorescence signal from donor and acceptor is time-averaged signature from microstate that occurs during a particular time of t in

the frame rate. We can also consider that a specific conformational state of HJ (macro-states) is an ensemble of several high-energy quasi-degenerate conformation (micro-state) of HJ, and thus signal generated from FRET dyes are ensemble average of microstates that lies within the time-space boundary of specific macro-state conformation of HJ.
We have calculated normalized PDF of FRET efficiency (Figure 7.6.B and 7.6.D) which gives nature of subset that is independent of both sample size and bin-size in histogram, by using the following equation,

$$p(E_{FRET}) = \sum_{j=1}^{M} A_j e^{\left[-(E_{FRET}-\langle E_{FRET}\rangle_j)^2/2\sigma_j^2\right]} \quad (7.3)$$

Where, A is the amplitude, σ is the standard deviation. We can consider that any specific conformational state of HJ that contains relatively large number of high-energy quasi-degenerate conformation will contribute significantly to the distribution of PDF. Figure 7.6.A shows three distinct macrostate derived from MD simulation where one conformer is with high FRET (S1, open), one with low FRET (S3, close) and third one with intermediate FRET efficiency (S2) values. We will define those macrostate as simply "state" or Sn (where n = 1-3). Kinetic network with different rate constates is also given in Figure 7.6.A. It was observed that normalized PDF can be divided into three parts in presence of both 50 mM and 200 mM Mg^{2+} ion. Essentially, we can say that HJ have 3-state kinetic network when transitioning conformations. Interestingly, the amplitude of S1 and S2 in the presence of 50 mM are nearly equal (40-45%), that is approximately 3.5 time higher than the same for S3 state, which may reflect that HJ prefers to stay in the closed conformation in presence of less positive ion. However, amplitude of S1 and S3 are nearly equal (13%) in the presence of high concentration of 200 mM Mg^{2+} ion, that is approximately 6 times less than the amplitude of intermediate FRET (S2, 75%) signifying population for S2. It may reflect the dynamic nature of negatively charged DNA in presence of high concentration of positive ion. Our experimental data is strongly supported by the MD simulation, which also found similar contribution from S1, S2 and S3.

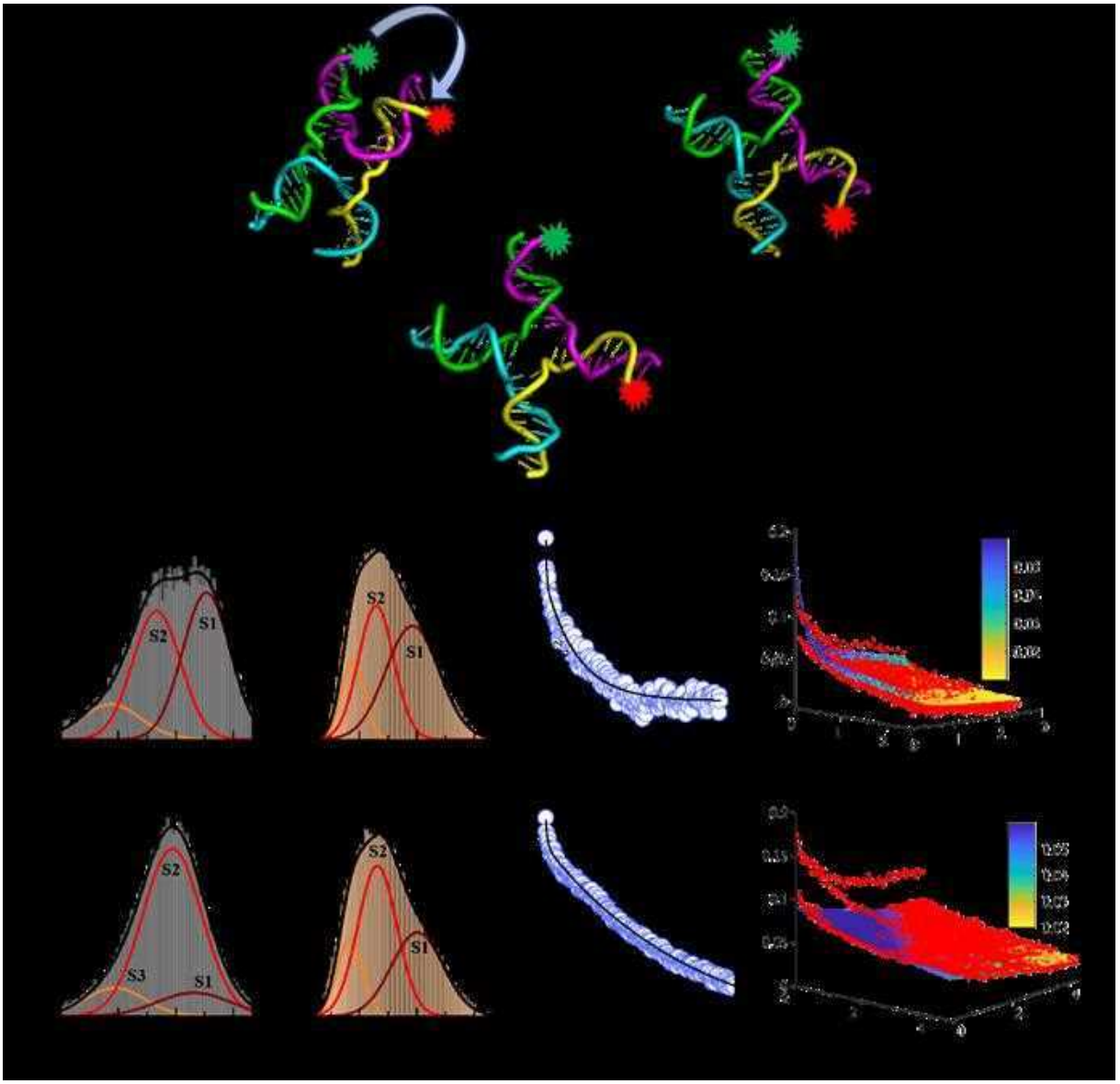


Figure 7.6 Effect of Mg^{2+} ion in FRET efficiency and conformational dynamics. (A) Three conformational structures of HJ captured in MD simulations – one with high FRET, one with low FRET and another with intermediate FRET. (B) Relative probability of experimental FRET efficiency histogram shows three prominent states at E_{FRET} = 0.25 (S3, orange), 0.5 (S2, red), and 0.76 (S1, Maroon) in presence of 50 mM Mg^{2+}. (C) Similarly, probability density of MD simulated time trajectories showing three conformational states in presence of 50 mM Mg^{2+}. (D) Two-point or 2nd order time correlation function (TCF) fitted with two exponential decay equation (black line) showing two decay constants in the presence of 50 mM Mg^{2+}. (E) Three-dimension plot of four-point or 4th order time correlation function at $\tau 2$= 0.05 s with fitting lines in presence of 50 mM Mg^{2+}. (F-I) Similar to Figure B to E, relative probability density plot of experimental and simulated FRET efficiency, decay of two-point time correlation function and four-point time correlation in presence of 200 mM Mg^{2+} are shown.

Table 7.2 Optimized Parameter for PDF of Three Macrostate.

Ion	A_1	$\langle E_{FRET}\rangle_1$	σ_1	A_2	$\langle E_{FRET}\rangle_2$	σ_2	A_3	$\langle E_{FRET}\rangle_3$	σ_3

50 mM	0.46 ±0.05	0.76±0.01	0.12 ±0.007	0.41±0.002	0.50±0.02	0.12 ±0.007	0.13±0.05	0.26±0.06	0.15±0.04
200 mM	0.13 ±0.02	0.69	0.19±0.01	0.75±0.02	0.58	0.16 ±0.002	0.12 ±0.007	0.28	0.16 ±0.009

7.3.3 Time Correlation Function (TCF) Formalism Describes the Rates and Time-Scale of Conformational Exchange in the 3-State Model of HJ

Dynamics and kinetic information of transitional exchange of HJ are characterized by TCF analysis of E_{FRET} time-trajectories. Two-point TCF are calculated from real-time smFRET fluctuation data using following equation,[279]

$$C(\tau) = \langle \partial E_{FRET}(0)\, \partial E_{FRET}(\tau) \rangle \quad (7.4)$$

Here, $\partial E_{FRET}(t) = E_{FRET}(t) - \langle E_{FRET}(t) \rangle$, where $\langle E_{FRET}(t) \rangle$ is the mean of E_{FRET} determined from time-trajectories data from a single-molecule and τ is the interval between two successive measurements. Interestingly, $C^2(\tau)$ has information about the minimum number of the macrostate or conformation available in the conformational exchange model, and kinetic information related to conversion from one macrostate to another. $C^2(\tau)$ can also be expressed as per the following equation, $C^2(\tau) = \sum_{i,j=1}^{M} \left[\partial E_{FRET_i} p_{ij}(\tau)\right] \times \left[\partial E_{FRET_i} p_i^{eq}\right]$, where p_i^{eq} is probability of presence of i^{th} macrostate present at equilibrium, $p_{ij}(\tau)$ is the conditional probability that HJ undergoes transition from i^{th}macrostate to j^{th}. As shown in the Figure 7.6.D and 7.6.H, the decay of TCF of HJ in the presence of 50 and 200 mM Mg^{2+} ion, both decay shows exponential in nature. However, TCF for 50 mM Mg^{2+} shows much faster decay at early interval times compared to the same for 200 mM Mg^{2+} presumably because of less electrostatic interaction in the solution. Decay of TCF is bi-exponential with longer-time of 3.8 s which is a major component with amplitude of 64%, and faster time component of 0.07 s which is a minor component with amplitude of 36%. Importantly, the number of exponential term in TCF dictates the minimum number of macrostate present in transitional exchange dynamics of HJ, which is $2 + 1 = 3$ that is alternative proof of presence three macrostate in conformation dynamics in addition of three-component PDF which is discussed Figure 7.6.B. We assign 0.07 second component as local chain dynamics and longer time of 3.8 seconds as macrostate interconversion time.

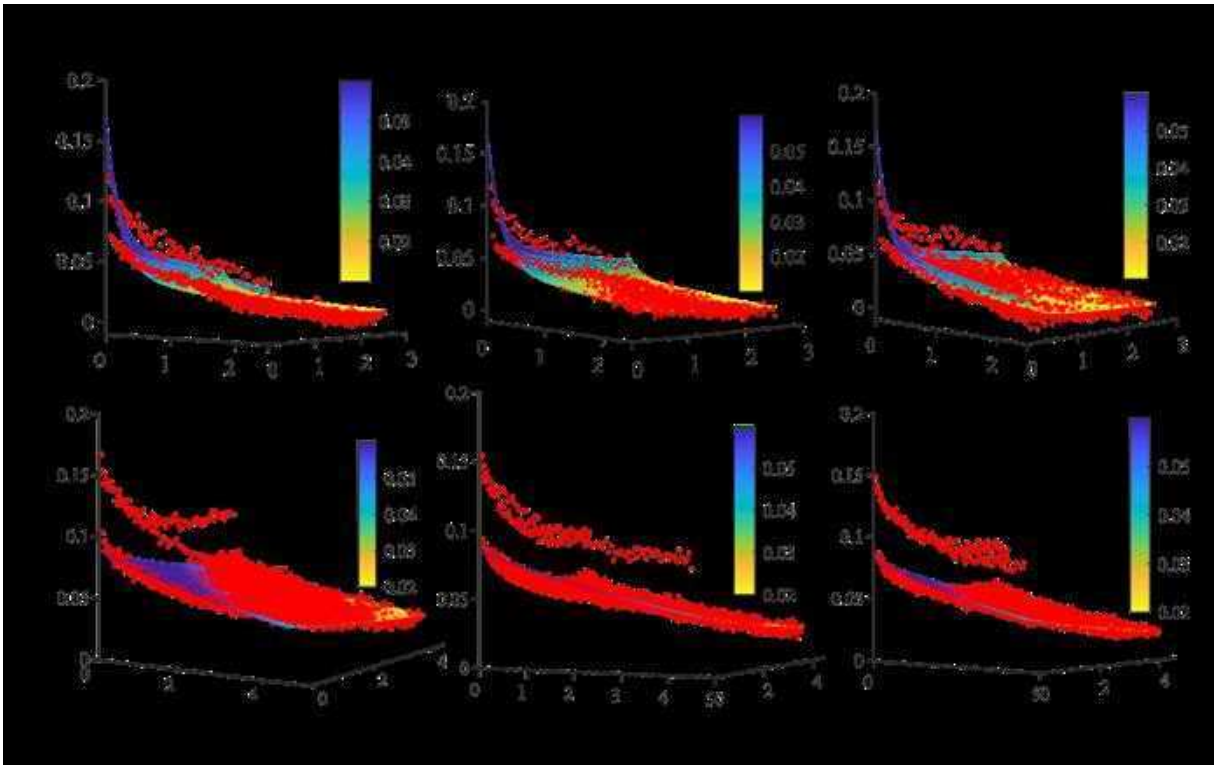


Figure 7.7 (A-C) Three-dimension plot of fourth order time correlation function at different waiting times 0.1 s, 0.25 s and 0.5 s, respectively, in the presence of 50 mM Mg^{2+}. (D-F) The three-dimension plot of the fourth order time correlation function at different waiting times 0.1 s, 0.25 s and 0.5 s respectively, in the presence of 200 mM Mg^{2+}.

Table 7.3 Time constant and amplitude calculated of the two-point time correlation function obtained from the biexponential fitting function.

Ion	A_1	τ_1 (s)	A_2	τ_2(s)
50 mM	0.36	0.181	0.64	3.787
200 mM	0.51	5.31	0.49	8.19

Table 7.4 Optimized Parameter for the 4th order time correlation function.

Ion	τ_2 (waiting time)	A_{22}	A_{23}	A_{32}	A_{33}	Root Mean square error
50 mM	0.05 s	0.0391	0.0361	0.0361	0.0754	0.0278
	0.1 s	0.0374	0.0318	0.0318	0.0698	0.0272
	0.25 s	0.0346	0.0315	0.0315	0.0712	0.0250

	0.5 s	0.0311	0.0302	0.0302	0.0737	0.0222
200 mM	0.05 s	0.0430	0.0191	0.0191	0.0104	0.0029
	0.1 s	0.0325	0.0200	0.0200	0.0164	0.0036
	0.25 s	0.0382	0.0173	0.0173	0.0126	0.0033
	0.5 s	0.0348	0.0154	0.0154	0.0171	0.0045

4th-order TCF can give us information about role of intermediate conformation in the kinetic pathway of HJ.[279] In Figures 7.6.E and 7.6.I shows three dimensional plot of 4th order correlation function decay when four successive data points separated by the interval τ_1, τ_2, and τ_3 of time average product, calculated by the following equation:

$$C^4(\tau_1, \tau_2, \tau_3) = \langle \delta E_{FRET}(0) \times \delta E_{FRET}(\tau_1) \times \delta E_{FRET}(\tau_1 + \tau_2) \times \delta E_{FRET}(\tau_1 + \tau_2 + \tau_3) \rangle \quad (7.5)$$

We find that the conformational dynamics of HJ go through a couple of interesting points which is described here for 50 mM Mg^{2+}. First, HJ go through high-FRET state (S1) to low FRET state through an intermediate state (S2). Conversion of high-FRET state to low FRET state (S3) through intermediate state is reversible but the conversion of low FRET to high FRET state is not reversible (Figure 7.6.A). The rate constant for conversion of high FRET state to intermediate state k_{12} and reverse transition k_{21} is almost equal, which is around 0.15 s^{-1} (Table 7.5). However the conversion of intermediate state to low FRET state k_{23} is more than three times faster than the same for high-FRET state to intermediate state. The HJ conformation returns back to intermediate state with much higher rate constant of 4.84 s^{-1} rather than directly interconversion to high FRET state (S1), which has much lower rate constant of 0.009 s^{-1}.

For the 200 mM Mg^{2+}, the fastest interconversion occurs for the macrostate S1 to S2 is 0.16 s^{-1}, while the backward transition from S2 to S1 have a rate constant of 0.02 s^{-1}. The interconversion between the S2 to S3 states is also the same as the S2 to S1 state at 0.02 s^{-1}, while the backward transition has a rate constant of 0.09 s^{-1}. The slowest interconversion process from S1 to S3 macrostate has rate constant of 0.003 s^{-1}; the reverse transition has rate constant of 0.014 s^{-1}. Overall, HJ conformation transition dynamics go through several structures and inter-conversion have complex kinetic network model.

7.3.4 Free-Energy Landscape of Conformational State Determining the Transition Barrier

Considering sum of all probabilities to unity, the free-energy (in k_BT) of HJ's specific conformation, j, can be written as a function of E_{FRET}, [271]

$$G_j(E_{FRET}) = -k_B T \ln\{p_j(E_{FRET})\} \quad (7.6)$$

$$= -k_B T \ln\left[p_j^{eq}/\sigma_j\sqrt{2\pi}\right] + k_B T\left[-(E_{FRET} - \langle E_{FRET}\rangle_j)^2/2\sigma_j^2\right] \quad (7.7)$$

And total free energy of all conformers is calculated from sum of all macro-state or HJ conformations, using following equation: $G(E_{FRET}) = -k_B T \ln\left[\sum_{j=1}^{M} p_j(E_{FRET})\right]$. From optimized rate constants described in the previous section, free energy of activation is calculated using the Arrhenius equation,[271]

$$G_{ij}^{0\#} = -k_B T \ln\left(\frac{k_{ij}}{k_{max}}\right) \quad (7.8)$$

According to the Arrhenius equation $k_{ij} = k_{max} e^{-G_i/k_B T}$. Here, the pre-exponential factor in the equation is considered to k_{max}. The fastest rate conversion in the HJ conformational transition between macrostates is corresponds to $k_{32} = 4.84\ s^{-1}$.For the purine-pyrimidine (G-C) nucleotides the activation barrier is ~2 kcal/mol which is equivalent to 3.4 $k_B T$.[274] So, the corrected pre-exponential factor $k_{max} = k_{32} \times e^{3.4} = 4.84 \times 30 = 145\ s^{-1}$. All other activation barrier values are calculated based on this value considering the fact that any interconversion between three macrostates involves either formation or disruption of secondary structure of DNA HJ that can lead to formation of many other macrostate or intermediate state which will not support our 3-state model mechanism.

Table 7. 5 Optimized Forward and Backward Rate Constant for DNA HJ.

Ion	k_{12} (s^{-1})	k_{21} (s^{-1})	k_{13} (s^{-1})	k_{31} (s^{-1})	k_{23} (s^{-1})	k_{32} (s^{-1})
50 mM	0.15	0.16	-	0.009	0.43	4.84
200 mM	0.16	0.02	0.003	0.014	0.02	0.09

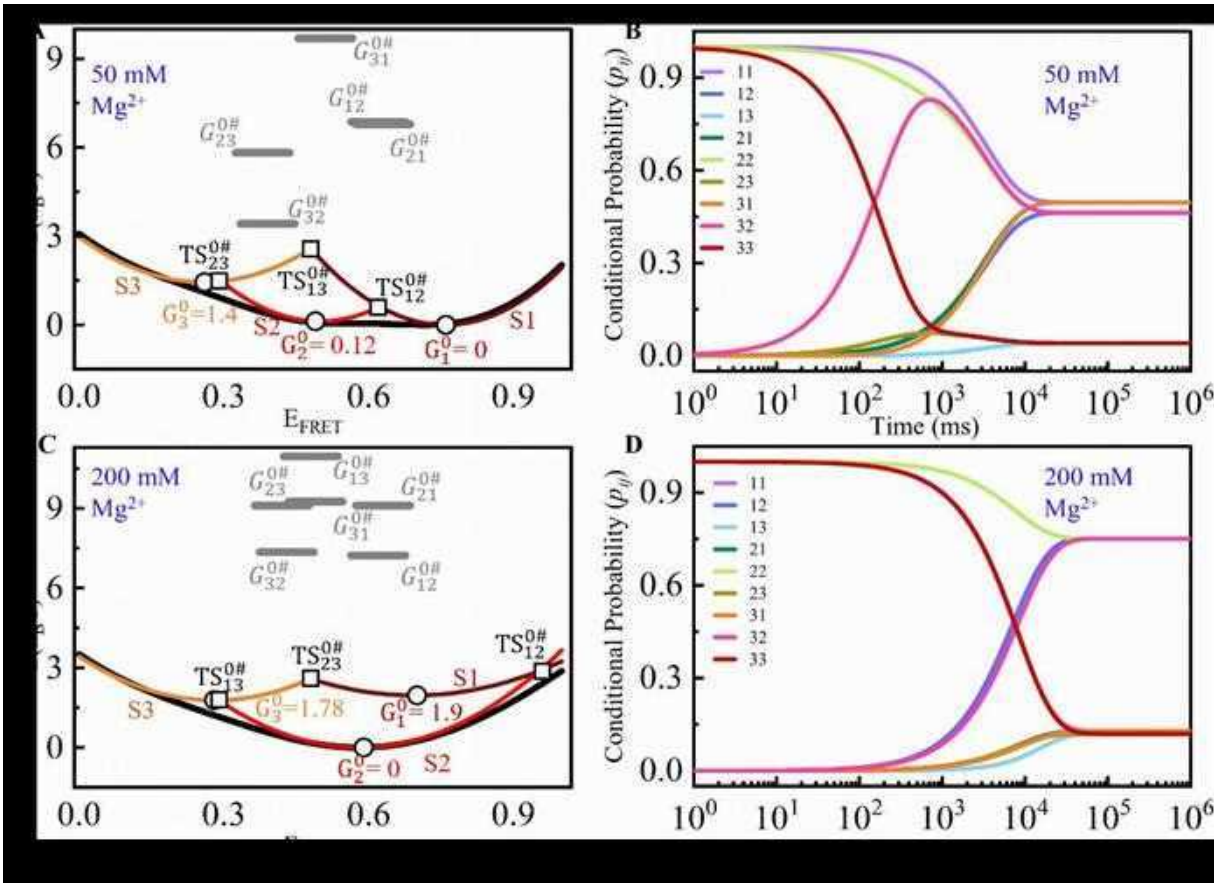


Figure 7.8 (A) Free energy G (k_BT) landscape for DNA HJ in presence of 50 mM Mg^{2+}. (B) The time-dependent conditional probabilities, p_{ij}, which give the likelihood of the system in presence of 50 mM Mg^{2+}. (C-D) Similar to Figure A-B, Free energy G (k_BT) landscape and the time-dependent conditional probabilities of 200 mM Mg^{2+} are shown.

Figure 7.8.A and 7.8.C shows the individual contribution of macrostate conformation to the free energy surface of DNA HJ, which is shown in three different colors (S1, Maroon; S2, Red; and S3, Orange). The sum or overall free-energy contribution is shown in black line. The individual contribution to free-energy of each conformation shown in parabola in presence of both 50 mM and 200 mM Mg^{2+} starting with $G_n = 0$ (ground state), where $n = 1 - 3$. In presence of 50 mM Mg^{2+}, $G_1^0 = 0\ k_BT$, $G_2^0 = 0.119\ k_BT$ and $G_3^0 = 1.44\ k_BT$, where superscript '0' represents that we have taken the minimum of macrostate S1 as reference to all other energies. Each macrostate/conformations also shows a parabolic nature of energy change with respect to E_{FRET} because we considered gaussian distribution of distance from one arm to another arms of HJ. This also describes the approximate relative probabilities for the occurrence of HJ configuration or macrostate that deviates from the mean values, and thus there is an entropic contribution associated with the conformational change. Gaussian shape of free energy accurately describes the nature of conformational dynamics of HJ because of branch shape and many probabilities of conformational states even with same FRET efficiency value. However, the non-zero gaussian shape for both case of 50 mM and 200 mM may be attributed to the stronger interaction and conformational state changes through specific macrostate over the time. The presence of three macrostate for each case is likely due to the presence of distinctly different distance between two HJ arms contributing from the existence of chain configurations, presence of different local arms flexibility etc. in presence of positive ions.

Table 7.6 Optimized Free Energy Minima and Transition Barrier Enthalpies for DNA HJ (all unit given in k_BT).

Ion	$G_{12}^{0\#}$	$G_{21}^{0\#}$	$G_{13}^{0\#}$	$G_{31}^{0\#}$	$G_{23}^{0\#}$	$G_{32}^{0\#}$	$H_{12}^{0\#}$	$H_{21}^{0\#}$	$H_{13}^{0\#}$	$H_{31}^{0\#}$	$H_{23}^{0\#}$	$H_{32}^{0\#}$
50 mM	6.86	6.78	-	9.69	5.82	3.40	6.25	6.17	-	7.13	4.35	1.92
200 mM	7.23	9.11	10.97	9.26	9.11	7.36	6.45	8.33	8.40	6.69	7.63	5.88

To find out the activation energy and enthalpic contribution (Table 7.6), we have used the kinetic rate model and Arrhenius equation, and the S1 → S2 state has very high activation energy, $G_{12}^{0\#} = 6.86\ k_BT$, and for the backward reaction, S2 ← S1 has a similar energy $G_{21}^{0\#} = 6.78\ k_BT$ for the transition in the presence of 50 mM Mg^{2+} ion. The most favourable transition we have found for the state S3 → S2 with low activation energy is 3.40 k_BT and the transition from S2 → S3 is 5.82 k_BT energy is required. The transition from S3 → S1 has required very high activation energy (9.7 k_BT), indicates a less favorable transition. The enthalpic contribution for the S2 → S3 state is 4.35 k_BT for the transition barrier ($G_{23}^{0\#} - G_2^0 = 5.72\ k_BT$), and for the backwards process, it has 1.92 k_BT ($G_{32}^{0\#} - G_3^0 = 2.04\ k_BT$), which is the most favourable one. Similarly, the activation energy for the conformational transition in the presence of 200 mM Mg^{2+} ion is in the range of approximately 7-11 k_BT.

The transition barrier for the S1 → S2 states is $G_{12}^{0\#} - G_1^0$ is 6.81 k_BT, and the enthalpic contribution for the same state is 6.25 k_BT. The backwards transition for the same states required a 6.17 k_BT enthalpic contribution higher by $G_{21}^{0\#} - G_2^0$ = 6.66 k_BT. The transition barrier of S3 → S1 states is also comparable with the S1-S2 states; it has the enthalpic contribution of 7.13 k_BT.

In order to estimate ensemble average quantities, it is utmost necessary to compute the equilibrium probability distribution of individual macrostates and conditional probabilities (p_{ij}) that determine the possibility of transition from state i to state j for our proposed three-state kinetic network model.[271] Probabilities can be obtained by solving the following master equation that includes a set of coupled 1st order ordinary differential equations depicting time dependent macrostate probabilities.

$$\dot{\mathbf{p}}(t) = \mathbf{k}\mathbf{p}(t) \tag{7.9}$$

$\mathbf{p}(t)$ denotes time-dependent macrostate probability vector where $\mathbf{k}$ is a 3×3 rate matrix.[271]

$$\mathbf{k} = \begin{bmatrix} -\sum_{i\neq j=1}^{M} k_{1j} & k_{21} & k_{31} \\ k_{12} & -\sum_{i\neq j=1}^{M} k_{2j} & k_{32} \\ k_{13} & k_{23} & -\sum_{i\neq j=1}^{M} k_{3j} \end{bmatrix} \tag{7.10}$$

Off-diagonal elements in rate matrix satisfy $k_{ij} = k_{ji}$ which means gain in population in macrostate j due to transition from i to j should be equal to the loss due to the transition in state i. Diagonal elements has been depicted as sum of all reactions that diminish population of i^{th} macrostate. In order to have such a master equation, time dependent macrostate probabilities must show completeness $\sum_{i=1}^{M} p_i(t) = 1$ and detailed balance $p_i^{eq} k_{ij} = p_j^{eq} k_{ji}$. Rate matrix $\mathbf{k}$ also satisfies a symmetry property that summation of each column of the rate matrix leads to zero which leads toward the first eigenvalue (λ_0) to be also 0 and the remaining ones are negative.

Given a particular set of rate constants, one can solve the master equation by obtaining eigenvalues and eigenvectors for each macrostate that satisfy $\mathbf{k}\nu_i = \lambda_i \nu_i$. Eigenvalues for a system denote the characteristic relaxation rates of the coupled equations and eigenvectors are the linear

combination of elementary transitions depicting a collective mode. We have obtained the Eigenvalues by fitting two point correlation function with bi-exponential as $C^2(\tau) = a_1 e^{\lambda_1 t} + a_2 e^{\lambda_2 t}$ when the general solution of the master equation has the form $p(t) = p^{eq} + c_1 v_1 e^{\lambda_1 t} + + c_2 v_2 e^{\lambda_2 t}$. Thereafter we optimize the rate matrix in order to achieve equilibrium probability in each macrostate and the corresponding eigenvalues obtained for the system of interest with Nelder-Mead optimization algorithm. Figure 7.8.B and 7.8.C plots time dependent conditional probabilities obtained from optimized rate and optimized solution to the master equation which eventually converges at $t \to \propto$ to equilibrium population (see Table 7.2; A_1, A_2 and A_3) in macrostates for ionic environment 50 mM and 200mM respectively.

Conditional probabilities represent likelihood of transition from state i to state j if the previous state at t = 0 is state i. We have obtained the equilibrium population in the macrostates in 10-100 s timescale.

7.3.5 Differential Mg^{2+} Adsorbance Dictate Conformational Exchange and Stability in HJ

To elucidate temperature dependent local ionic environment around DNA HJ, we turned toward appropriately calibrated (See Methods and Figure 7.1) structure-based coarse-grained simulations aiming to quantify the adsorbance of positively charged Mg^{2+} ions on DNA HJ backbone. In our structure-based CG model, temperature range 0.5-0.6 in reduced units matches the simulated RMS fluctuations to experimental B-factors at room temperature.[295-296] This suggests temperature range 0.42-0.5 ε/k_B is equivalent to room temperature and essentially corresponds to 50-60 K in Gromacs[286] units.

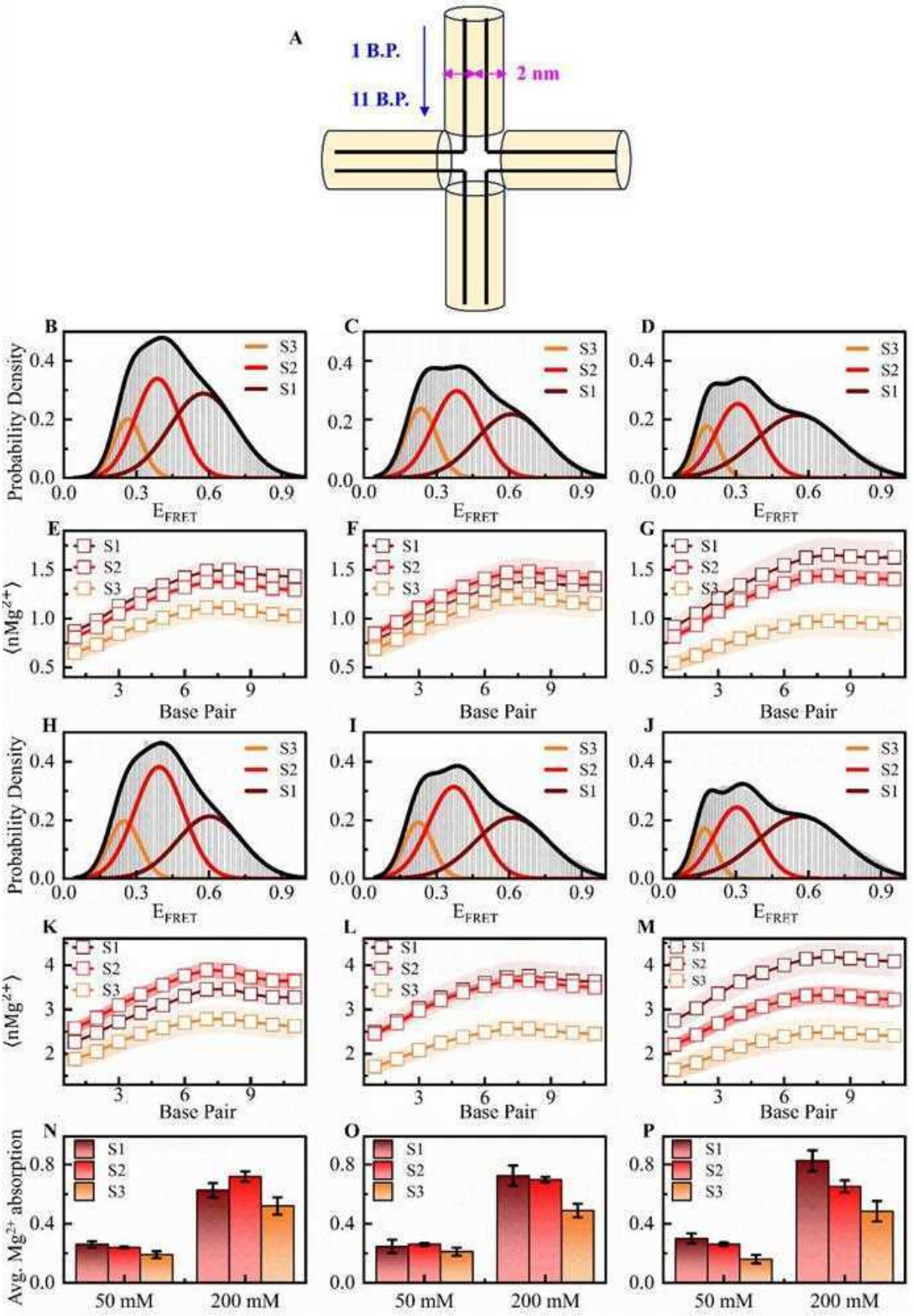


Figure 7.9 (A) Schematic representation of Mg^{2+} deposition along chain in 1 nm cylinder around each double strand. B.P. means base pair. (B-D) Probability Density of FRET efficiency calculated from the MD simulation trajectory shows three prominent states corresponding to $\mathbf{E_{FRET}}$ in presence of 50 mM Mg^{2+} ion at 60K (In our structure-based CG model 60K represents experimental room temperature), 75K and 90K

respectively. (E-G) Represents number of Mg^{2+} along chain in 1nm cylinder around each double strand of HJ at 60K, 75K and 90K respectively in either state 1 (high FRET), 2 (intermediate FRET) or 3 (low FRET) in presence of 50 mM ion concentration. (H-J) Probability Density of FRET efficiency calculated from the MD simulation trajectory shows three prominent states corresponding to $\mathbf{E_{FRET}}$ at in presence of 200 mM Mg^{2+} Ion 60K, 75K and 90K respectively. (K-M) Represents number of Mg2+ along chain in 1nm cylinder around each double strand of HJ at 60K, 75K and 90K respectively in either state 1 (high FRET), 2 (intermediate FRET) or 3 (low FRET) in presence of 200 mM ion concentration. (N-P) Represents the average Mg^{2+} absorption (50 and 200 mM Mg^{2+}) for each double strand in each state 60K, 75K and 90K respectively.

Mg^{2+} adsorbance on DNA HJ surface has been quantified by the scheme described in Figure 7.9.A. A cylindrical structure has been considered along each DNA duplex strand, while the axis of the cylinder has been placed at the line containing the center of masses of complementary backbone nucleotides in the duplex strands. Adsorbance of Mg^{2+} ions has been quantified upto a distance 1 nm in contrast to 6-7 Å that all-atom explicit solvent model predicts for counter ion absorption. The ionic environment along HJ and its correlation to the microstate stability has been probed for Gromacs temperature 60-90 K. Figure 7.9.(A-C) plots simulated probability density of FRET efficiency between a virtual donor and acceptor tagged at chain C and chain D ends respectively for temperatures 60K, 75K, and 90K respectively at 50 mM explicit Mg^{2+}.At such moderate ion concentration, significant repulsion between negatively charged HJ strands at conformational states aligns with the effect of temperature to facilitate conformational exchange between macrostates.

While S1 and S2 are fairly populated than S3 at T* = 60 K, relative population of S1 in comparison to S2 and S3 enhances at higher temperatures (B-C). As temperature rises, a shoulder is prominent at high-FRET regime. In addition, gradual broadening of S1 has been observed indicating enhanced conformational freedom in that macrostate due to rise in temperature.

To understand the correlation between stability of individual macrostates with their local ionic environment, we compute average number of Mg^{2+} (nMg^{2+}) along the scheme detailed above at 50 mM divalent $MgCl_2$ (Figure 7.9.(E-G)). We have observed significant spatial heterogeneity in Mg^{2+}-DNA phosphate backbone interaction at HJ surface. As one moves toward the junction center from strand ends, each nucleotide-pair seems to interact with larger number of Mg^{2+} ions and adsorbance is maximum at junction center due to very high charge density (Figure 7.9 (E-G)).

Relative absorption at different macrostates (shown with Gaussians in (Figure 7.9.(B-D)) has been quantified from the structural parameters and is well correlated with the populations at such moderate ion concentration. Macrostate S1 and S2 have significantly higher Mg^{2+} count on DNA surface at all the temperatures than S3 and is in conformity with the population distribution at Figure 7.9.(B-D) and Figure 7.10.

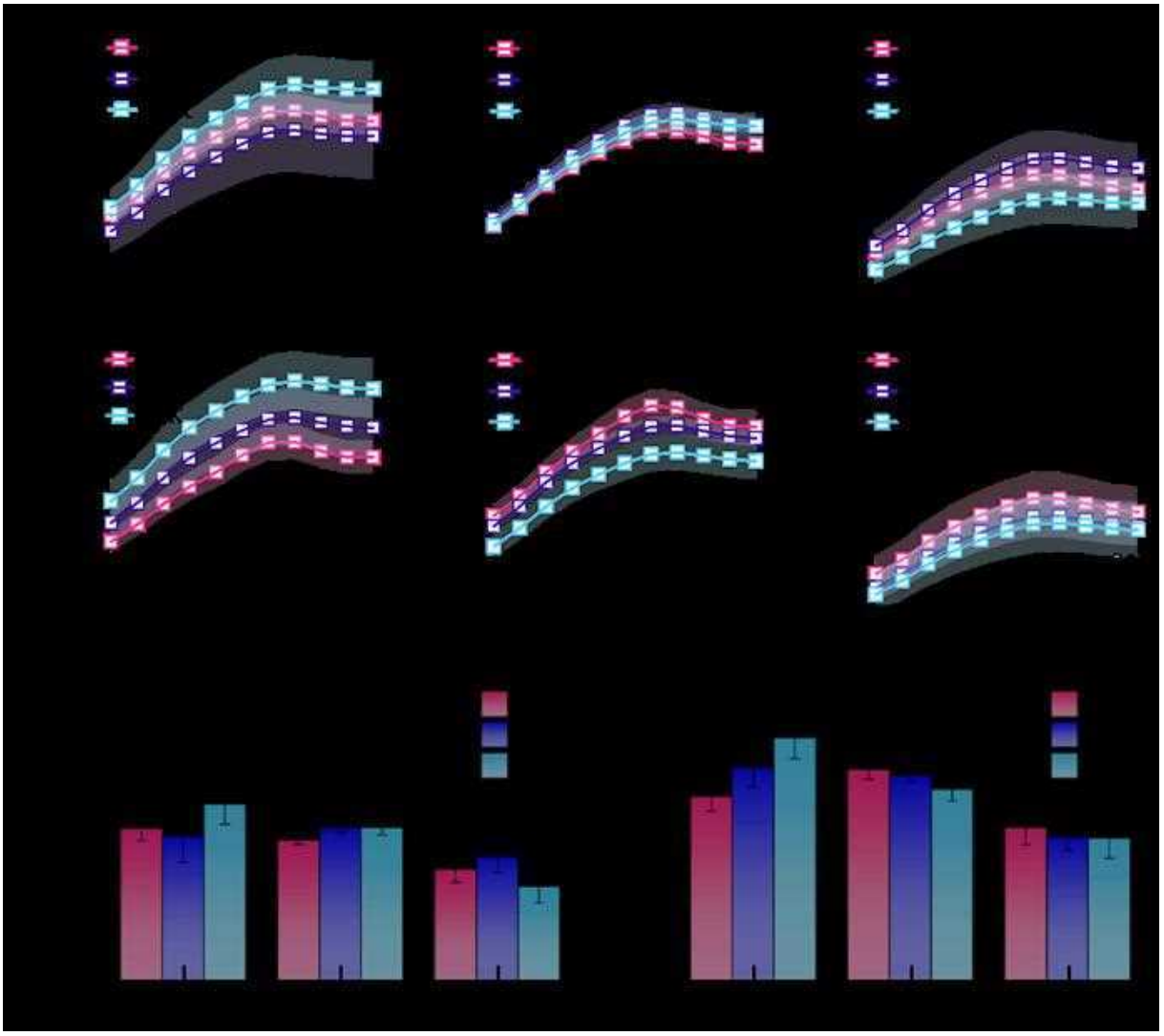


Figure 7.10 (A-C) Represents the number of Mg^{2+} vs the number of base pairs along the chain in a 1nm cylinder around each double strand of HJ in the presence of 50 mM Mg^{2+} concentration at 60K, 75K and 90K in state 1 (S1), State 2 (S2) and State 3 (S3) respectively. (D-F) Represents the number of Mg^{2+} vs the number of base pairs along the chain in a 1nm cylinder around each double strand of HJ in the presence of 200 mM Mg^{2+} concentration, at 60K, 75K and 90K in state 1(S1), State 2 (S2) and State 3 (S3) respectively. (G-H) Represents the average Mg^{2+} absorption for each double strand at 60K, 75K and 90K in State 1 (S1), State 2 (S2) and State 3 (S3), respectively, at 50 and 200 mM Mg^{2+}, respectively.

At such moderate ion concentration, due to enhanced interaction with Mg^{2+}, conformational ensemble of S1 gains stability due to reduction of inter-strand repulsion interactions, At near physiological ion concentration (200 mM), conformational state S2 having an unstacked conformation is the predominant one at low temperature (T*=60K) due to excessive counter-ion condensation on DNA surface that switches the negatively charged DNA inter-strand repulsion to a counter-ion mediated positively charged strand repulsion in the stacked S1 state (Figure 7.9.H and Figure 7.9.(K-M) at different temperatures namely 60K, 75K and 90K). Such positive counterion condensation mediated inter-strand repulsion is highest in S3 and S1 due to stacked conformation. Hence S2 is the most probable conformation with lowest such inter-strand repulsions with significantly high Mg^{2+} absorption. At significantly higher temperatures, enhancement of population in conformational state S1 appears due to increased fluctuations can overcome such barrier of conformational exchange due to repulsion between S2 and S3 (Figure 7.9. (H-J)). Average adsorbance of Mg^{2+} per nucleotide in different conformational states at 50 and

200 mM has been shown in Figure 7.9.(N-P) at different temperatures. At higher ionic strength, asorbance of Mg^{2+} on DNA HJ nucleotides enhances by a factor of 2 leading toward counter-ion mediated repulsions.

Here, we would like to summarize our discussion and interpretation based on observation from experimental data. The interpretation of the data in terms of 3-state model is primarily based on the time constants in the time correlation function analysis as well as three gaussian functions in overall PDF. As a macrostate is composed of multiple microstates and macrostates are formed based on the energy distributions among microstates, we can assume that this three-state model not only interpretation of the data that we have acquired using our microscope with the resolution limit. Therefore, we can state that the dynamics interconversion may go through multiple numbers of intermediate states which possibly with high energy. An experiment and interpretation of the data from the single molecule intensity time-trajectories always has a limitation based on the experimental setup. The interconversion rate and dynamics that are acquired by our setup has a time-resolution of 50 ms. However, the dynamic change or interconversion of DNA HJ can go through multiple states and multiple intermediate state which are beyond the resolution of our setup. Exact characterization of thermodynamic parameters for existing microstates of DNA HJ and role of Mg^{2+} are key question in our study which give an interpretation that Mg^{2+} concentration gradually increases towards the center of junction. This observation opens up various follow-up questions in relation to the exact mapping of Mg^{2+} ion with oppositely charged phosphate backbone of DNA, and relation of charge density with thermodynamically stable macrostate.

7.4 Conclusion

In conclusion, our study elucidates the intricate dynamics of DNA HJ and critical role of ionic environment in modulating their conformational that are extremely difficult to characterize by ensemble averaged experimental techniques. By combining sophisticated optical methods of smFRET with MD simulations, we have identified three distinct thermodynamically stable conformational macrostate and demonstrated that transition rates between these states are significantly influenced by the divalent ion concentration. The predominance of open conformational state under physiological condition highlights the importance of ionic stabilization in HJ dynamics. Additionally, our observation of differential divalent ion concentration in the central region of HJ underscores the junction points pivotal role in governing conformational stability and genetic recombination. In future, further study on other biologically relevant ions and DNA repair process could help understand molecular mechanism of regulatory processes and give more comprehensive knowledge on the relationship of structure-function-dynamics. Ultimately, our study will contribute to a more detailed understanding of heterogeneous genome maintenance which is a key feature of nature as well as genome repair process, potentially informing the development of therapeutic strategies targeting genetic disorders. Previous reports predominantly highlighted conformational transitions between isoI and isoII forms or concentrated on force-field-dependent stabilization of stacked states; however, our study identifies a significant open state under physiological Mg^{2+} concentrations and uncovers distinct ion localization patterns, particularly at the junction center. This observation addresses a significant knowledge gap by correlating local ion distribution with macrostate stability. These findings underscore the significance of ionic microenvironments in determining the free-energy landscape of DNA junctions and provide opportunities for additional investigation into how specific ion types or sequence variants affect DNA structure-function interactions in recombination and repair mechanisms. This may also give us an indication with evidence from experimental and MD simulation on how life is created with so much genetic diversity.